RSC Advances

ROYAL SOCIETY OF CHEMISTRY

www.rsc.org/advances

Journal Name

ARTICLE

Activated Nanoporous Carbon-Gold Nanoparticle Composite Electrode with Enhanced Volumetric Capacitance

Received 00th January 20xx,
Accepted 00th January 20xx

DOI: 10.1039/x0xx00000x

www.rsc.org/

David Avila-Brande[a,*], Daniel Arenas-Esteban[a], L. Carlos Otero-Díaz[a], Andrés Guerrero-Martínez[b], Gloria Tardajos[b], Javier Carretero-González[c,*]

The novel and straightforward preparation route of an activated nanoporous carbon, produced from abundant biomass, containing a fine dispersion of gold nanoparticles whitin the carbon microstructure and its application as supercapacitor electrode material is presented. A remarkable increase of the volumetric capacitance value, respect to the activated nanoporous electrode without gold nanoparticles, was observed. Interestingly, the electrochemical series resistances of the symmetric cell decreased up to one order of magnitude in comparison with the unmodified carbon material. The incorporation of gold nanoparticles overcomes the characteristic irreversible charge storage of activated carbon electrodes containing surface oxygenated groups. All these findings pave the way to a novel synthetic route of highly-dense carbon nanocomposites for the design of new electrode architectures with potential application in electrical double-layer capacitors development.

Introduction

The increase in energy consumption, projected to be double by 2050, together with the depletion of the conventional resources, based on fossil fuels, and the impact that their overuse causes in the climate change, have led governments to invest in finding alternative sources of renewable and sustainable energy[1]. The intermittent nature of these fonts of energy (i.e. sun and wind) makes necessary storing the exceeding electricity[2]. Efforts are focused especially on the development of electrochemical energy storage systems like batteries and supercapacitors that should meet market requirements such as low cost, efficiency and safety[3].

In particular, electrical double-layer capacitors (EDLC) store charge at the electrode/electrolyte interface by ion adsorption on the surface of a porous carbon electrode. EDLC can achieve high gravimetric capacitance values ~ 100-200 F g^{-1} because of the high specific surface area of electrode materials and the very small charge separation between the surface atoms from the electrode and the ions from the electrolyte (typically below 1 nm)[4]. Because of the way EDLC store charge can be fully charged in a matter of seconds to minutes with power densities exceeding those of batteries; however, their energy density, in general about 5 Wh kg^{-1}, is at least ten times lower than in batteries. Recently, some strategies to adapt supercapacitors to energy requirements (target value ~ 20-30 Wh kg^{-1}) have been offered by employing neutral aqueous electrolytes that led wider cell voltage[5] or hybridizing the supercapacitor cell either by using an inherent battery-type electrode[6] or by adding a small concentration of redox-active molecules to the electrolyte[7].

In order to achieve high gravimetric energy and power densities, EDLC electrode materials must possess a large specific surface area (SSA) (~ 1500 m^2 g^{-1}) available for ion electrosorption, pore size distribution (PSD) optimized for the desired combination of energy and power characteristics, good electrical conductivity, and wettability by the electrolyte[8]. Thus, advancing the synthesis of nanoporous carbons appears to be crucial among the approaches to adapt EDLC to high energy demanding applications. Different synthetic approaches to produce porous carbon materials, such as activated carbons (ACs), carbide derived carbons, mesoporous templated carbons, carbon nanotubes, carbon onions, carbon aerogels, and graphene, have been developed[9]. However at present most of the commercial EDLCs are based on activated carbons due to their well-developed manufacturing technologies, easy production in large quantities, relatively low cost and great cycle stability[10,11].

Most ACs has been synthesized from precursors based on the fossil fuels, but the shortage of these resources requires finding affordable and renewable new types of precursors. In recent years, many different natural materials such as wood, bamboo, coconut

[a] Department of Inorganic Chemistry, Faculty of Chemistry, Universidad Complutense de Madrid, E–28040, Madrid, Spain.
[b] Department of Physical Chemistry, Faculty of Chemistry, Universidad Complutense de Madrid, E–28040, Madrid, Spain.
[c] Polymer Ionics Research Group, Department of Inorganic Chemistry and Solid State Technology, Chemical Faculty, Warsaw University of Technology, Noakowskiego 3, PL-00664 Warsaw, Poland

† Electronic Supplementary Information (ESI) available: Thermo-gravimetric analysis (TGA, black) and the differential temperature curve (DTG, red) of CAC-AuNPs; Schematic diagram of two AuNPs in which an interdigitated bilayer of oleylamine separates adjacent nanocrystals, Pulsed Electrochemical Impedance Spectroscopy (PEIS) for the symmetric supercapacitor cell made with CAC and CAC-AuNPs nanoporous carbon electrodes
. See DOI: 10.1039/x0xx00000x

shell or olive pits have been reported for the preparation of ACs[12-16].

Although recent research has been focusing on using abundant and renewable sources of nanoporous carbon electrodes, for application areas like vehicles and portable electronics improving the volumetric performance of the electrodes at high charge/discharge rate is at a premium[17]. In this sense volumetric capacitance values comparable to those exhibited by RuO_2 has recently been achieved for carbon-based electrode materials like titanium carbide[18] and graphene derived electrode materials[19].

The final capacitance values will be affected by several parameters like surface area, average pore size, pore size-ion size relations and the electrochemical series resistance (ESR), among others. Then, a careful evaluation of these parameters will need it in order to achieve a suitable electrochemical performance. For instance, both electrolyte and active electrode material resistance contribute to the ESR of the cell. Regarding the former, the conductivity of the electrolyte ions inside the carbon nanopores at high rates is much more reduced than across the separator and the active electrode macropores[20]. Therefore, appropriate ion-size and pore-size interactions might be crucial to cycle supercapacitors at high current densities with acceptable capacitance retention. The distortion of the ion-solvation shell or even the loss of some of the solvent molecules surrounding the ions facilitates the accommodation of the ions inside narrow pores and then the enhancement of capacitance[21]. Recently, it has been also observed the existence of an optimum pore size for each ion with regards to rate capability[15]. Related to the ohmic resistance of the activated nanoporous carbon electrode, this can substantially be reduced by the incorporation of other carbon additives such as carbon black, graphite or carbon nanotubes[22] or a low cost and excellent conductor such as copper nanocrystals[23]. Though copper is more economic than noble metals such as gold or platinum and yield also higher volumetric capacity and contribute also to the increase of energy storage through the presence of faradaic reactions, is easily oxidized into CuO in the form of nanoparticles, with a dramatic decrease of the electronic conductivity from 108 S/m into 0.1-1 S/m[24]. Therefore, gold may offer an excellent alternative to copper as main composition of nanoparticles within ACs matrices. In this context, gold nanoparticles (AuNPs) have been synthesized in CDCs through wet chemical synthesis of nanocrystals in aqueous solution[25]. However, due to the inherent difficulties of dispersabilities of hydrophobic ACs in water, and considering the advances of synthesis of gold nanoparticles in non-aqueous solvents[26], we consider interesting the use of organic solvents to obtain highly loaded ACs-AuNPs matrices with promising electronic conductivities. In addition the intrinsic conductivity of the electrode materials is also affected by the presence of oxygen groups at the carbon surface[27] as well as the synthesis conditions (i.e. temperature of carbonization, method of activation)[28].

Herein, for the first time, we report a facile an efficient synthetic method to incorporate gold nanoparticles in an activated nanoporous carbon matrix, in organic solvent, derived from an abundant natural plant resource: the Guadua Angustifolia bamboo specie as it is graphically depicted in Scheme 1. This precursor has been selected, since the obtained AC, exhibits a specific capacitance of 154 F/g, matching and even surpassing the values quoted in the literature for AC derived from lignocellulosic precursors[29]. However, the specific capacitance markedly decreases due not only to the presence of surface oxygenated acidic groups[30] but also the low electronic conductivity of activated carbon being in order of 10 to 100 S/m[31, 32]. The precursor is first carbonized and then chemically activated by KOH during thermal treatment. Then AuNPs have been incorporated to the carbon matrix by using a method for the large-scale synthesis of organoamine-protected AuNPs[33]. Consequently, a nanostructured CAC-AuNPs material is obtained exhibiting a microstructure composed of highly disordered and entangled graphene layers with a 25% of Au inside and decorating the surface.

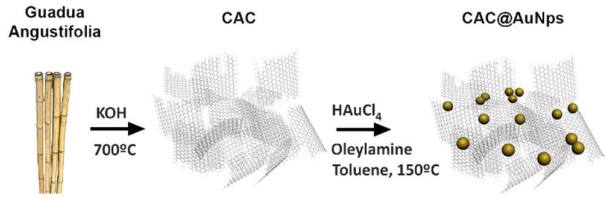

Scheme 1. Schematic illustration of the chemical synthesis of CAC-AuNPs composite, in which the carbon obtained from Guadua Angustifolia is initially chemically activated by an impregnation method, and subsequently loaded by AuNPs synthesized in organic media.

The incorporation of a more dense material like gold in the AC provoked an enhancement of almost double of the volumetric capacitance values (47 F cm^{-3}) in aqueous electrolyte as well as the drop of one order of magnitude of the internal resistance of the supercapacitor cell. The change in the textural properties of the activated nanoporous carbon upon addition of gold nanoparticles and the reliable synthesis method of these metal-nanoporous carbon composites suggest the possibility of production of many different nanostructured composite electrode materials for electrochemical energy storage applications.

Experimental Section

Synthesis of the Activated Carbon-Gold nanoparticles (CAC-AuNPs) composite electrode.

Prior the carbonization, the lignocellulosic precursor Guadua Angustifolia, was reduced to 1 cm length. 5 gr of these particles were placed into a quartz crucible and heated at 400 ºC during ten minutes in a tubular furnace under Ar atmosphere in order to remove their low boiling and melting point organic compounds. Finished the carbonization process, heating was turned off and the system was cooled down to 25 ºC.

The carbon obtained from the previous stage was chemically activated with KOH by using the impregnation method. A solution of 10 ml containing 10 M KOH and the carbon in weight ratio 4:1 was stirred at 70ºC during 120 min. The resulting slurry was later on dried at 110 ºC followed by a thermal activation carried out in a tubular furnace under Ar atmosphere, during 60 min at 700 ºC. Elapsed the activation time, heating was turned off and the system

was cooled until 25 ºC. The activated carbon was washed in a 0.1M HCl solution and with distilled water until the total elimination of chlorine ions (detected via precipitation method with $AgNO_3$ 1 M solution). The final product was dried in a furnace at 110 ºC during 24h.

For the preparation of the final CAC-AuNPs composite, 70 mg of the activated carbon were dispersed by sonication (15 minutes) in 10 mL of toluene, and subsequently mixed with 3.25 mL of oleylamine (OAm) and 35 mg of $HAuCl_4 \cdot 3H_2O$. The mixture was stirred during 12 hours at room temperature, to allow complete diffusion of chemicals within the carbon matrix. The mixture was heated to reflux at 150 ºC during 2 hours. Then at room temperature, the mixture was centrifuged and cleaned twice with toluene (2500 rpm, 10 min) to remove excess of OAm, and the precipitate was redispersed in 0.5 mL of toluene. Finally, the CAC-AuNPs sample was heated under vacuum at 80ºC during 1 week to remove traces of solvent.

Material characterization

Scanning electron microscopy (SEM) micrographs were obtained with a JSM 6335 F electron microscope operating at 10 kV and a working distance of 15 mm. Transmission electron microscopy (TEM) studies have been performed in a JEOL 3000 F (acceleration voltage of 300 kV) microscope (point resolution of 1.7 Å). The Infrared (IR) spectra were recorded on a FTIR Thermo Nicolet200 spectrometer with samples as KBr pellets in the 4000–400 cm^{-1} region. Thermogravimetric analysis (TGA) and differential thermal analysis (DTA) were performed on a TA Instruments apparatus (SDT Q600 model) using O_2 atmosphere. The sample was heated at 5 ºC min^{-1} up to 900 ºC. Textural characterization was made by means of N_2 adsorption isotherms at 77 K using Surface Area and Porosity Analyzer ASAP2020 (Micromeritics). The specific surface area (SBET) was calculated according to BET theory and the micropore volume using the linearization of the Dubinin-Radushkevich (DR) equation[34]. The pore size distributions (PSD) were calculated by using the SAEIUS software for the 2D non-local density functional theory (2D-NLDFT) considering energetically heterogeneous to the pore walls of the standard carbon slit-shape pore geometry[35], this approximation was also used to calculate de surface area (SDFT < 50 nm) and the microporous surface area (SDFT <2 nm) being the latter the main contribution of nanopores.

Electrochemical characterization

The electrodes were prepared by mixing 95 wt% of carbon material with 5 wt% of polytetrafluoroethylene solution (PTFE 60wt%, Sigma-Aldrich) as polymer binder. The mixture was hand-mixed with few milliliters of ethanol until viscous slurry was obtained. The slurry was laminated with the help of a glass test tube until the final thickness was within 250 - 200 micrometer range. Then, the film was dried and kept at 120 ºC under vacuum for 12 hours prior to each measurement. Electrodes of comparable mass (up to 15 mg and density of 0.29-0.30 g cm^{-3} and 0.65-0.70 g cm^{-3} for the CAC and CAC-AuNPs electrodes, respectively) and 11 mm in diameter were assembled in a symmetric Swagelok-type cell, wetted with the electrolyte, separated with a glass fiber membrane (Whatman® glass microfiber filters, grade GF/B) of 12.7 mm in diameter and placed in direct contact with titanium plungers.

Electrochemical studies were performed in an aqueous solution of 6 M potassium hydroxide (pellets 85%; Flucka Chemical Corp.) in a voltage window ranging from 0 to 1 V. Electrochemical cyclic voltammetry (CV) at different scan rates (from 1 to 50 $mV.s^{-1}$) as well as galvanostatic measurements at different current densities ranging from 0.1 to 3 $A.g^{-1}$ were performed at ambient conditions with a multichannel potentiostat/galvanostat (Biologic VMP3, France). The specific capacitance was evaluated per active mass of a single electrode after a minimum of 10 cycles was recorded at each scan rate. Pulsed Electrochemical Impedance Spectroscopy (PEIS) measurements were carried out by applying a low sinusoidal amplitude alternating voltage of 10 mV to the cell at frequencies from 1 MHz to 10 mHz using the above mentioned multichannel potentiostat/galvanostat. Measurements were performed at open circuit voltage (OCV).

The specific capacitance (C_{grav}) was calculated from the CVs at each scan rate using the following equation

$$C_{grav} = \frac{2I}{\frac{dV}{dt}m} \quad (1)$$

Where I (A) is the current, m (g) the mass of the active material and dV/dt ($mV\ s^{-1}$) is the scan rate. From galvanostatic curves, specific capacitance was calculated (after a minimum of 5 cycles) by using the same equation 1 but in this case I/m corresponds to the current density and dV/dt to the slope extracted from the galvanostatic discharge curve after ohmic drop subtraction. Volumetric capacitance was obtained by multiplying gravimetric capacitance by the density of the electrode.

Results and discussion

Bamboo waste is selected as raw material because it´s a renewable biomass, it has a high content of carbon (see elemental analysis in Table 1), yields a high quality active carbon and its low cost (abundance).

Table 1. Elemental analysis from the precursor and the CAC (%).

	C	H	N	O
Guadua angustifolia	44.84	5.84	0.91	48.41
CAC	82.85	2.88	1.22	13.05

As it can be seen in Figure 1a, the pieces of the raw dried bamboo are formed by fibers since is mainly composed of cellulose, lignin and hemicellulose. A close inspection of the raw material by Scanning Electron Microscopy (SEM) reveals the fibrous nature of the precursor (see Figure 1b).

Generally, a carbonization process at 400ºC is needed to enrich the carbon content by eliminating non-carbon species, followed by a chemical activation process with KOH at 700ºC to enhance the pore volume, enlarge the diameter of pores and increase the porosity. The success of the activation process is reflected in the doubled carbon content above 80% in the chemical activated carbon (CAC) from Guadua Angustifolia compared with the raw material (see Table 1). Moreover, the SEM image of CAC displayed in Figure 1c clearly shows how the chemical activation modifies the surface of the raw material due to the elimination of volatiles. Notice that the material is composed by fibrous particles showing almost exfoliated very thin carbon flakes and the development of a high amount of pores. The chemical composition of CAC, displayed in Table 1, exhibits a concentration of oxygen and hydrogen of 13.05 % and 2.88 % respectively, suggesting the presence of surface oxygenated acidic and hydroquinone/quinone groups that can be responsible of pseudo-capacitance in the carbon material.

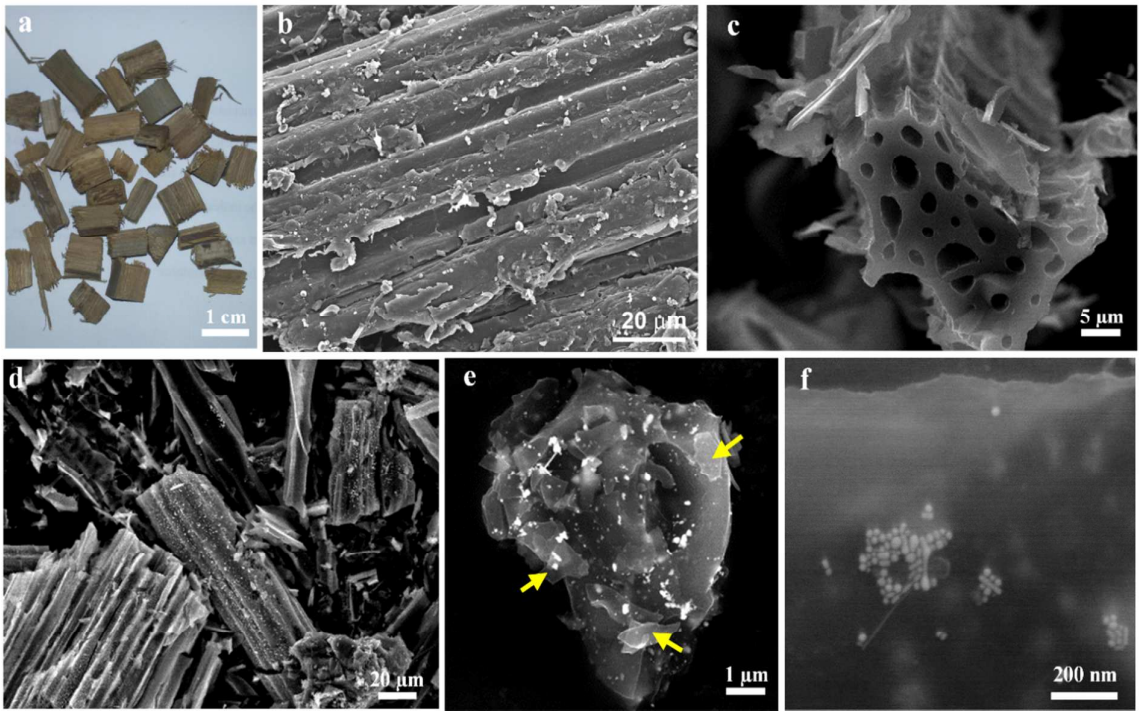

Figure 1: a) Photograph of the dried bamboo pieces before the carbonization b) SEM image of the precursor before and c) After carbonization and chemical activation d) Low magnification SEM image of CAC-AuNPs composite material e) Image of a single particle where the brightest contrast clearly demonstrates the presence of AuNps f) High magnification image of a wall of CAC-AuNPs showing ordered arrangements of AuNps on the surface of the CAC, in addition the blurred bright areas correspond to AuNps located inside the CAC.

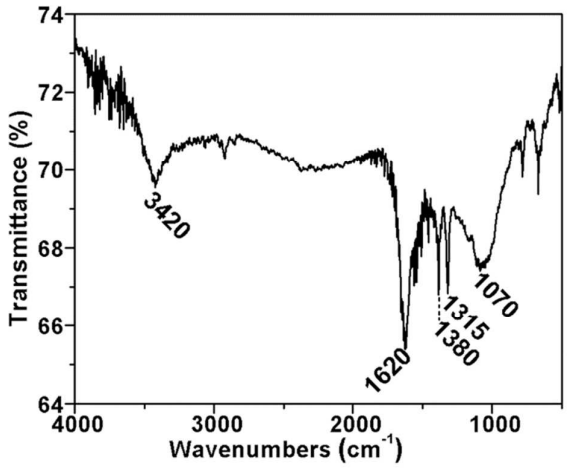

Figure 2: Infrared spectrum of CAC

The analysis of the infrared spectrum (Figure 2) allows the identification the different groups. The sharpest band at 1620cm^{-1} indicates the presence of quinonic groups ν(C=O), whereas those situated at 1315 and 1380 cm^{-1}, due to the C–O stretching, reveals the formation of xantenes ν(C–O) and ethers ν(C–O) groups. The single band at 1070 cm^{-1} reveals that the ethers groups are symmetric (R – O – R). Finally, the broad band at 3240 cm^{-1}, due to the H–O stretching, confirms also the presence of phenolic groups $\nu_{(H-O)}$ and the weak and broad bands in the range from 2850 – 2950 cm^{-1}, can be assigned to the asymmetric $\nu_{as(C-H)}$ and symmetric $\nu_{s(C-H)}$ C–H stretching.

Oleylamine (OAm) is common reagent used in the synthesis of stable and monodisperse nanoparticles[36]. In fact, the synthesis of Au nanoparticles is very simple since only involves OAm and $HAuCl_4$ in an organic solvent. Here, OAm acts not only as reduction agent of Au^{3+} into Au, but also stabilizes grow of the particles through the affinity of the NH_2 group with the metal. Under these synthetic conditions, it seem feasible that a highly porous structure of an

active carbon such as CAC, can act as a nanoreactor where the Au-OAm nanoparticles can be growth yielding an interesting composite CAC-AuNPs (see Scheme 1). The success of this approximation is clearly demonstrated by the SEM images displayed in Figure 1d,e,f. The image displayed in Figure 1d shows a perspective of the CAC-AuNPs composite material where all the particles are decorated by areas with brighter contrast corresponding to the Au nanoparticles. At higher magnification (Figure 1e) a single particle of this material is displayed containing a substantial amount of Au nanoparticles. The most important point is that in those areas the Au nanoparticles are not agglomerated but well-ordered as it can be observed at the high magnification SEM image displayed in Figure 1f. Here, we note that the size of the nanoparticles on the surface is not homogeneous, but are well separated by around 2 nm, which is the length of the OAm molecule[37] In addition, the blurred bright contrast observed can indicate that also groups of particles are located inside the carbon material.

To further investigate the structure of the prepared composite material CAC-AuNPs, a HRTEM study has been performed. Figure 3 displays the HRTEM images at different magnification of this composite material. At low magnification (Figure 3a) we observe a very thin layer of active carbon containing darker areas where the Au nanoparticles have grown, exfoliated in the crushing of the microparticles observed by SEM during the TEM sample preparation. In fact some of these layers are marked by yellow arrows in Figure 1e. At higher magnification (Figure 3b) we detect the presence of single but also groups of particles with different size in the surface and inside the carbon layer with a separation between the closest particles ~2 nm (Figure 3c). The HRTEM images of single Au nanoparticles reveal that their size varies between 15 and 50 nm, and a multiply twinned structure (Figure 3d), which is typical for noble metals with a face-centered cubic structure at small sizes[38]. The amount of gold incorporated to the CAC has been analyzed by thermo-gravimetric analysis of a portion of CAC-AuNPs in air (see †ESI Figure SI1) yielding a loss of carbon of 75% and therefore a content of gold of 25%.

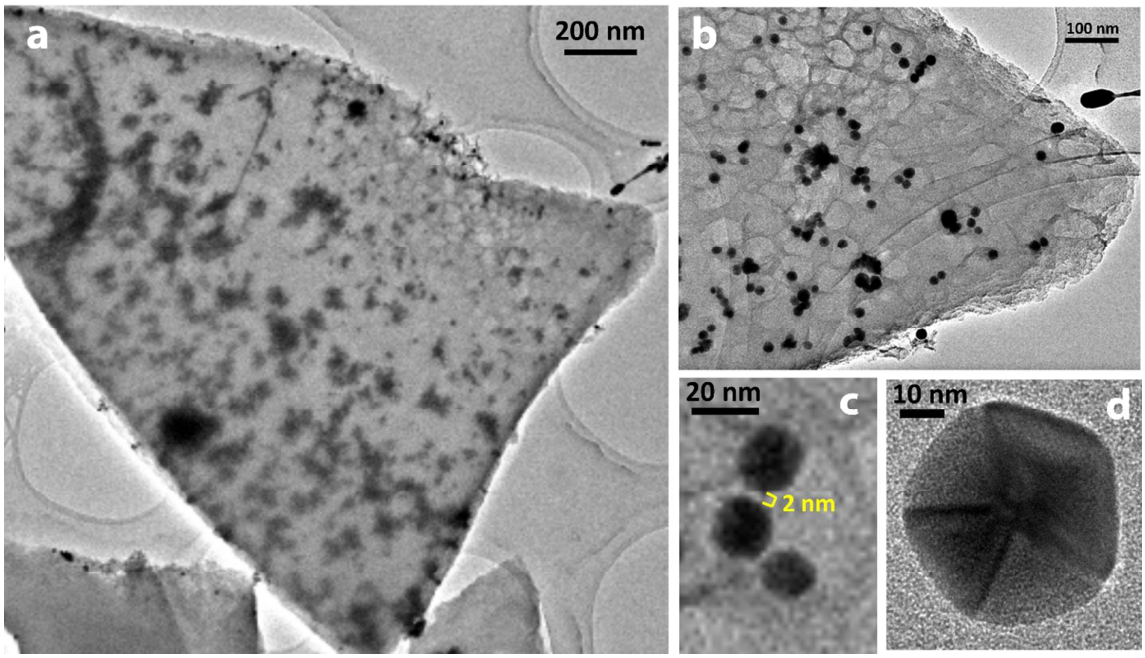

Figure 3: a) Low magnification TEM image of the composite material CAC-AuNPs, where the darker areas reveal the presence of AuNps. b) Magnified area from a) where isolated and ordered AuNps are clearly identified. c) Group o AuNPs showing an interparticle distance of 2 nm d) Single pentatwined Au nanocrystal.

The effect on the porous structure with the loading of AuNPs, has been study by the N_2 adsorption–desorption measurements at 77 K on the CAC and the composite material CAC-AuNPs prepared in this work. The isotherm plots of both materials depicted in Figure 4a follow the Type I according to the IUPAC classification[39]. It appears that the porosity consists mainly of micropores (width < 2 nm). The BET surface (S_{BET}) area and the micropore volume of CAC are one order of magnitude larger than in CAC-AuNPs, as effect of the loading of AuNPs (see Table 2).

Table 2. Textural properties of CAC and CAC-AuNPs

	S_{BET} (m^2/g)	$V_{micro\ (DR)}$ (cm^3/g)	$L_{0\ (DR)}$ (nm)	S_{DFT} (<2nm) (m^2/g)	S_{DFT} (<50nm) (m^2/g)	$L_{0\ (DFT)}$ (nm)	$L_{max\ (DFT)}$ (m^2/g)
CAC	2019	0.78	1.6	1657	1794	0.98	0.57; 0.91; 1.77
CAC-AuNPs	265	0.09	1.7	183	211	0.80	0.78

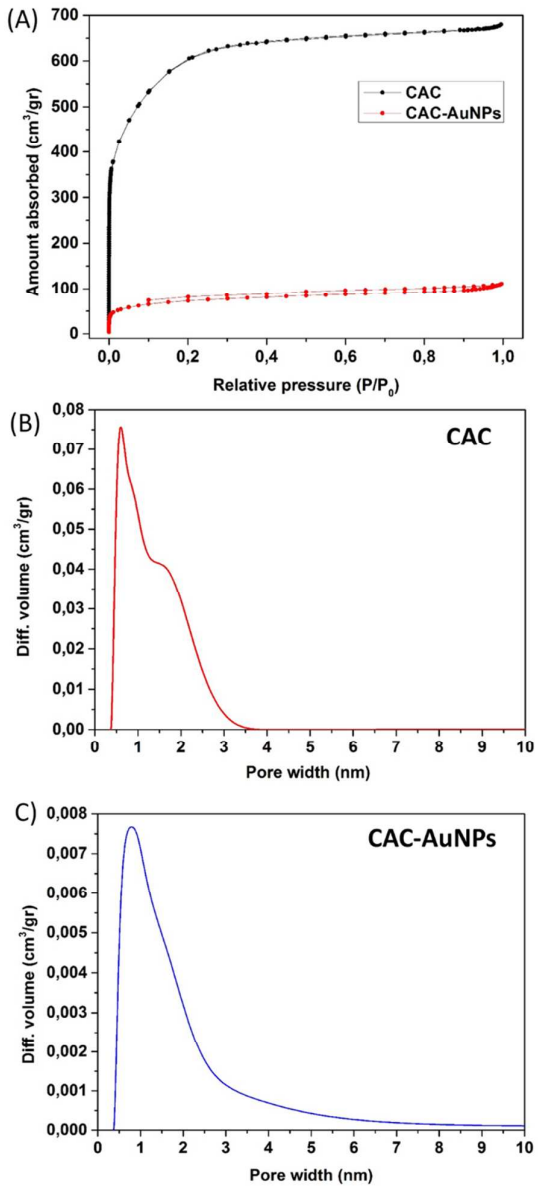

Figure 4: a) Comparison of the N2 adsorption/desorption isotherm plots from CAC and CAC-AuNPs. Pore size distributions of b) CAC and c) CAC-AuNPs.

The pore size distribution curves of both materials (see Figures 4b,c) show a similar trend, however whereas the curve of CAC present a maximum value at 0.57 nm and two well defined shoulders centred at 0.91 and 1.77 nm respectively, in the PSD of CAC-AuNPs the maximum is displaced at 0.78 nm and the shoulders disappear due the fact that the ratio of pores with a size between 1.5-2.5 nm are increased respect to smaller pores. Interestingly, the new pore distribution matches the size of the chain length of OAm at the surface of the AuNPs[40]. Therefore, we have analysed the typical interparticle distance between AuNPs by HRTEM (Figure 2c.) that has been determined in ~2 nm, showing an interdigitation of the monolayers of OAm between adjacent nanocrystals within the carbon matrix. (see ✝ESI Figure SI2). This result can be correlated to the increase of the pores with a size between 1.5-2.5 nm observed in the pore size distribution (see Figure 4c).

Figure 5 shows the cyclic voltametric response of the carbon electrodes containing gold nanoparticles (CAC-AuNPs) and without (CAC) recorded in a supercapacitor cell at 5 mV s^{-1} at room temperature in a symmetric two-electrode cell configuration. Both samples shown CVs with rectangular shape, typical of a capacitive behavior. Figure 5A shows higher gravimetric capacitance values for CAC (100 F g^{-1}) than the sample CAC-AuNPs (73 F g^{-1}). This is because of the presence of higher specific surface (2019 m^2 g^{-1} against 265 m^2 g^{-1}) in CAC than CAC-AuNPs[41,42]. However, sample CAC-AuNPs shows superior volumetric capacitance values (47 F cm^{-3}) in comparison to CAC (29 F cm^{-3}) as a consequence of the incorporation on its microstructure of gold nanoparticles as it shown in Figure 5b.

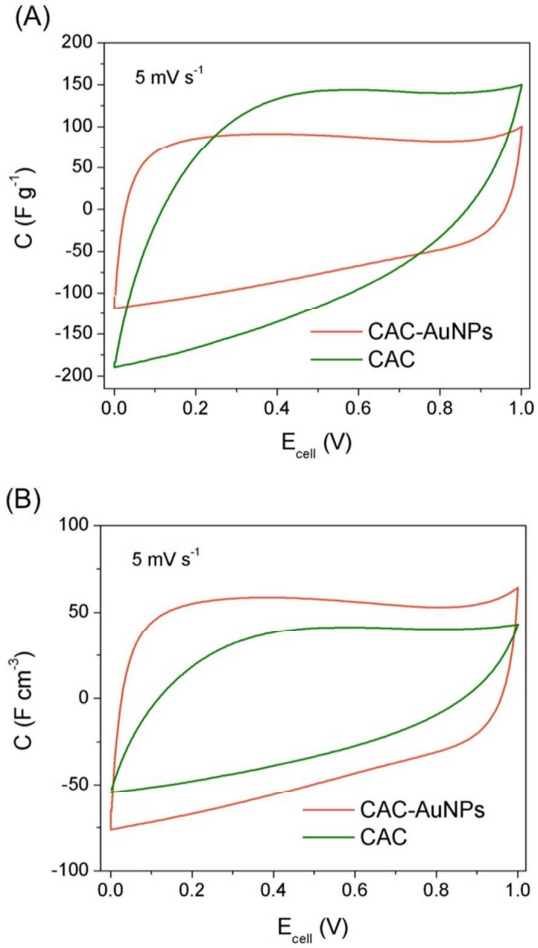

Figure 5: Cyclic Voltammograms of activated carbon sample with gold nanoparticles (CAC-AuNPs) and without (CAC). Comparison between the variation of the gravimetric (A) and volumetric capacitance (B) with the cell potential in 6 M KOH electrolyte. (Scan rate = 5 mV s-1)

Additional electrochemical measurements performed on the samples CAC-AuNPs and CAC in 6 M KOH electrolyte are shown in Figure 6. Figure 6a shows CVs at different scan rates for CAC-AuNPs

sample. The increasing of the ohmic resistance in the bulk electrolyte with increasing the scan rate produced a small distortion in the CVs. The distortion of the electrochemical response was more pronounced in CAC sample in which a highly resistive behavior during polarization can be observed in Figure 6b. The origin of this distortion could be due to the intricate diffusion of the ions inside the pores. However, the textural properties exhibited by both samples comprised the presence of a large amount of micropores accompanied by certain mesoporosity that should be optimum for retention of the capacitive properties as the sweep rate increase[20]. In addition, both samples presented enough micropore surface area SDFT (<2nm) (see Table 2) that should allow the accommodation of the electrolyte´s ions while cycling up to 1 V without the presence of sieving effect features[43] .

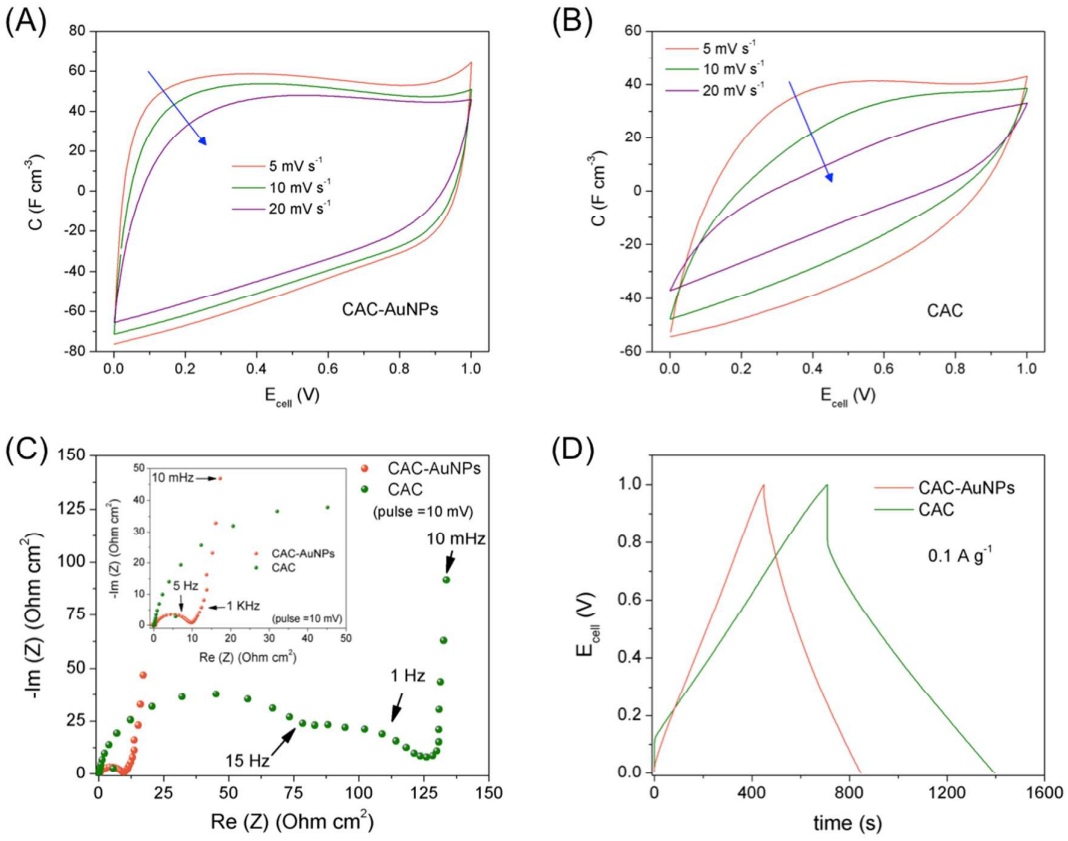

Figure 6: a-b) Cyclic Voltammograms at different scan rates for CAC-AuNPs (a) and CAC (b) samples. Pulsed electrochemical Impedance spectroscopy for CAC-AuNPs and CAC. Inset: Region at high frequencies showing the bulk electrode resistance of the CAC-AuNPs electrode. (d) Galvanostatic charge-discharge plots for CAC and CAC-AuNPs at 0.1 Ag^{-1}.

Therefore, the distortion might not be only due to the diffusion limitation of the ions into the nanopores but possibly to the presence of a high electrode resistance. The inherent electronic conductivity of the active electrode material is included in the equivalent series resistance (ESR). Then, it would be also possible by impedance spectroscopy analysis to further ascertain the role of functional groups and the inhomogeneous nanoporosity in the ohmic drop of the cell[44]. Figure 6c shows the Nyquist plot of the supercapacitor cell obtained from PEIS data. The vertical increase of the imaginary part of the impedance in both carbon electrodes confirms the capacitive nature of the electrochemical storage. The first semicircle of CAC sample is attributed to the bulk impedance while the second one appearing at lower frequencies suggests the parallel existence of a charge transfer resistance. Thus, it might be possible that faradaic reactions (irreversible) from the presence of functional groups at the surface of the activated carbon are at the origin of the high values of capacitance observed for sample CAC. We have compared both PEIS data before and after cycling for CAC supercapacitor cell evidencing the disappearance of the interfacial contribution which it was most probably due to the oxygen groups at the surface of the porous carbon (see ✝ESI Figure SI3). The total interfacial resistance at open circuit voltage is shown to be comparable than the bulk resistance and it was therefore evident how the presence of gold nanoparticles suppressed this effect, which is important for practical applications. The electrochemical series resistance (ESR) measured for CAC-AuNPs reaches the value of 8-Ohm cm^2, one order of magnitude lower that for sample CAC with an ESR value of 130-Ohm cm^2. Moreover, high electrochemical stability for the nanoporous carbon-gold nanoparticles electrode material was evidenced by PEIS measurements of the supercapacitor cell after cycling (see ✝ESI Figure SI4). From these measurements, we can also infer that an optimum interaction between carbon surface and gold nanoparticles was achieved. Figure 6d show the galvanostatic charge/discharge cycles at 0.1 A g^{-}

[1]. The charging discharging profiles show linear-like dependencies of the potential versus time in agreement with the capacitive charge-storage mechanism and the capacitance obtained from cycling voltammetry.

Conclusions

In summary, a facile and reproducible new method for the synthesis of activated nanoporous carbon-gold nanoparticles composites has been detailed. This approach yields nanostructured electrode materials with high-volumetric capacitance in aqueous electrolyte (6M KOH). Interestingly the suppression of the irreversible capacitance caused by the presence of oxygen moieties at the surface of the carbon has also been evidence after gold nanoparticles incorporation into the carbon matrix. The present results are of high significance because bring the possibility to fabricate nanoporous carbon-metal composites with a high potential of being used as the next generation of electrode materials in electrochemical energy storage applications.

Acknowledgements

The authors would like to thank the financial support through the projects with references MAT2013-44964-R (Spanish MINECO) and S2013/MIT-2753 (Comunidad de Madrid). A.G.-M. acknowledges receipt of a Ramón y Cajal Fellowship from the Spanish MINECO.

Notes and references

1 Deciding the Future: Energy Policy Scenarios to 2050 Executive Summary World Energy Council (2007).
2 G. L. Soloveichik, *Annu. Rev. Chem. Biomol. Eng.*, 2011, **2**, 503.
3 M. Winter and R.J. Brodd, *Chem. Rev.*, 2004, **104,** 4245.
4 B. E. Conway, Electrochemical supercapacitors – scientific fundamentals and technological applications, Kluwer Academic/Plenum Publishers, 1999.
5 K. Fic, G. Lotan, M. Meller and E. Frazckowiak, *Energy Environ. Sci.*, 2012, **5**, 5842.
6 G. G. Amatucci, F. Badway, A. D. Pasquier and T. Zheng, *J. Electrochem. Soc.*, 2001, **148**, A930.
7 S. Roldán, C. Blanco, M.Granda, R.Menéndez and R. Santamaría, *Angew. Chem. Int. Ed.*, 2011, **50**, 1699.
8 Y. Zhai, Y. Dou, D. Zhao, P. F. Fulvio, Ri. T. Mayes and S. Dai, *Adv. Mater.* 2011, **23**, 4828.
9 P. Simon and Y. Gogotsi, *Acc. Chem. Res*,. 2013, **46**, 1094.
10 A. Burke, *Electrochimica Acta*, 2007, **53**, 1083.
11 L. Wei, M. Sevilla, A. B. Fuertes, R. Mokaya and G. Yushin, *Adv. Energy Mater.*, 2011, **1**, 356.
12 A.W.M. Ip, J.P. Barford and G. McKay, *Bioresource Technology*, 2008, **99**, 8909.
13 C. Long, D. Qi, T. Wei, J. Yan, L. Jiang and Z. Fan, *Adv. Funct. Mater.*, 2014, **24**, 3953.
14 H. Wang, Z. Xu, A. Kohandehghan, Z. Li, K.Cui, X. Tan, T. J. Stephenson, C. K. King'ondu, C. M. B. Holt, B. C. Olsen, J. K. Tak, D. Harfield, A. O. Anyia and D. Mitlin, *ACS Nano*, 2013, **7**, 5131.
15 E. Redondo, J. Carretero-González, E. Goikolea, J. Ségalini and R. Mysyk, *Electrochimica Acta*, 2015, **160**, 178.
16 A. M. Navarro-Suarez, J. Carretero-González, V. Roddatis, E. Goikolea, J. Ségalini, E. Redondo, T.Rojo, and R. Mysyk, *RSC Adv.*, 2014, ***4***, 48336.
17 L. Wei and G. Yushin, *Nano Energy*, 2012, **1**, 552.
18 M. Ghidiu, M. R. Lukatskaya, M. Q. Zhao, Y. Gogotsi and M. W. Barsoum, *Nature*, 2014, **516**, 78.
19 X. Yang, C. Cheng, Y. Wang, L. Qiu and D. Li, *Science*, 2013, **341**, 534.
20 Y. Maletin, V. Strelko, N. Stryzhakova, S Zelinsky, A. B. Rozhenko, D. Gromadsky, V. Volkov, S. Tychina, O. Gozhenko and D. Drobny, *Energy and Environment Research*, 2013, **3**, 156.
21 C. Largeot, C. Portet, J.Chimiola, P. L. Taberna, Y. Gogotsi and P.Simon, *JACS*, 2008, **130**, 2730.
22 C. Portet, P.L. Taberna, P. Simon and E. Flahaut, *Journal of Power Sources*, 2005, **139**, 371.
23 L. Zhang, S. L. Candelaria, J. Tia, Y. Li, Y. Huang and Gu. Cao, *Journal of Power Sources*, 2013, **236**, 215.
24 Y. K. Jeong and G. M. Choi, *J. Phys. Chem. Solids*, 1996, **57**, 81.
25 J. J. Niu, V. Presser, C. J. Karwacki and Y. Gogotsi, *Mater. Express*, 2011, **1**, 259.
26 Y. Xia, Y. Xiong, B. Lim and S. E. Skrabalak, *Angew. Chem. Int.*, 2009, **48**, 60.
27 V. Ruiz, C. Blanco, E. Raymundo-Piñero, V. Khomenko, F. Béguin and R. Santamaría, *Electrochimica Acta*, 2007, **52**, 4969.
28 A. Linares Solano, *Chapter 1. Carbon Activation by alkali Hydroxides*, Chemistry and Physics of Carbon Edited by Ljubisa R. Radovic, Vol. 30. 2008, CRC Press.
29 P. González-García, T.A. Centeno, E. Urones-Garrote, D. Ávila-Brande and L.C. Otero-Díaz, *Applied Surface Science*, 2013, **265**, 731.
30 T.A. Centeno and F. Stoeckli, *Electrochimica Acta*, 2006, **52**, 560.
31 M. F. El-Kady, V. Strong, S. Dubin and R. B. Kaner, *Science*, 2012, **335**, 1326.
32 J. Sánchez-González, F. Stoeckli and T. A. Centeno, *Journal of Electroanalytical Chemistry*, 2011, **657**, 176.
33 H. Hiramatsu and F. E. Osterloh, *Chem. Mater.*, 2004, **16**, 2509.
34 F. Stoeckli, M.V. López-Ramón, D. Hugi-Cleary and A. Guillot, *Carbon*, **39**, 1103.
35 J. Jagiello and J. P. Olivier, *Adsorption*, 2013, **19**, 777.
36 S. Mourdikoudis and L. M. Liz-Marzán, *Chem. Mater.*, 2013, **25**, 1465.
37 J. Borges, J. A. Ribeiro, E. M. Pereira, C. A. Carreira, C. M. Pereira and F. Silva, *Journal of Colloid and Interface Science*, 2011, **358**, 626.
38 X. Lu, H. Y. Tuan, B. A. Korgel and Y. Xia, *Chem. Eur. J.*, 2008, **14**, 1584.
39 S. J. Gregg and K. S. W. Sing, *Adsorption, surface area and porosity*, Academic Press, London, 1982.
40 Z.Wanga, X. Wen, R. Hoffmannb, J. S. Son, R. Li, C. Fang, D.-M. Smilgiesa and T. Hyeon, *PNAS*, 2010, **107**, 17119.
41 E. Raymundo-Piñeiro, K. Kierzek, J. Machnikowski and F. Béguin, *Carbon*, 2006, **44**, 2498.
42 O. Barbieri, M. Hahn, A. Herzog and R. Kötz, *Carbon*, 2005, **43**, 1303.
43 R. Mysyk, E. Raymundo-Piñeiro, J. Pernak and F. Béguin, *J. Phys. Chem.*, 2009, **C113**, 13443.
44 B. E. Conway, *Impedance Behavior of Electrochemical Supercapacitors and Porous Electrodes in Impedance Spectroscopy Theory, Experiments and Applications* Wyley, 2005.

